Article

Cell Reports

Direct Lineage Reprogramming Reveals Disease-Specific Phenotypes of Motor Neurons from Human ALS Patients

Graphical Abstract

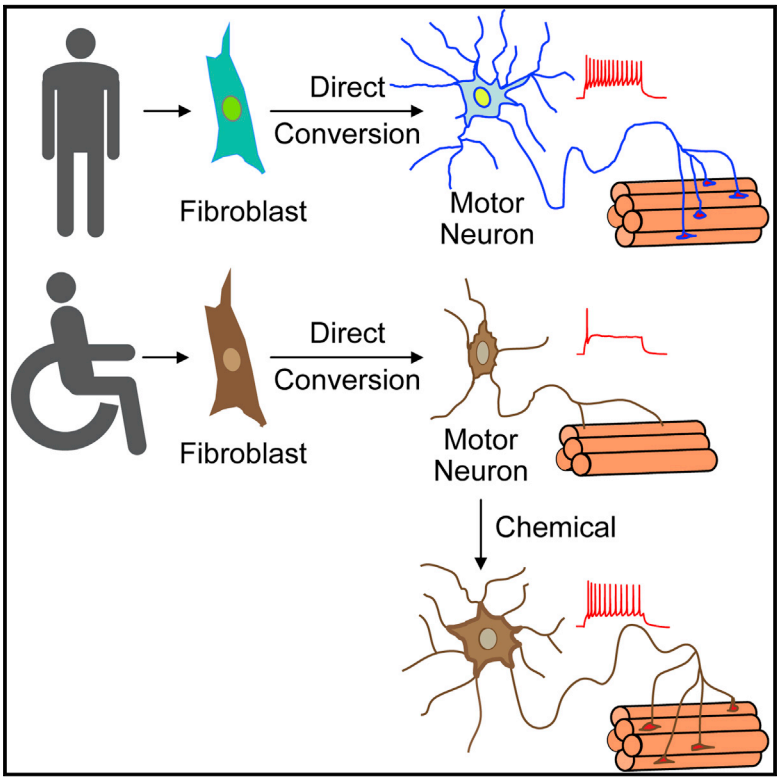

Authors

Meng-Lu Liu, Tong Zang, Chun-Li Zhang

Correspondence

chun-li.zhang@utsouthwestern.edu

In Brief

Liu et al. demonstrate that adult human fibroblasts can be efficiently and directly reprogrammed into highly pure spinal motor neurons (hiMNs). These neurons exhibit mature electrophysiology, form neuromuscular junctions, and control muscle activity. Interestingly, hiMNs from ALS fibroblasts show physiological deficits, which can be ameliorated by a small chemical compound.

Highlights

- Directly convert adult human fibroblasts to highly pure hiMNs
- hiMNs are physiologically mature controlling muscle activity
- hiMNs derived from ALS patient fibroblasts show pathophysiology
- Pathophysiology of ALS hiMNs can be rescued by a small molecule

Liu et al., 2016, Cell Reports *14*, 115–128
January 5, 2016
http://dx.doi.org/10.1016/j.celrep.2015.12.018

CellPress

Cell Reports
Article

Direct Lineage Reprogramming Reveals Disease-Specific Phenotypes of Motor Neurons from Human ALS Patients

Meng-Lu Liu,[1,2] Tong Zang,[1,2] and Chun-Li Zhang[1,2,*]
[1]Department of Molecular Biology, University of Texas Southwestern Medical Center, 6000 Harry Hines Boulevard, Dallas, TX 75390, USA
[2]Hamon Center for Regenerative Science and Medicine, University of Texas Southwestern Medical Center, 6000 Harry Hines Boulevard, Dallas, TX 75390, USA
*Correspondence: chun-li.zhang@utsouthwestern.edu
http://dx.doi.org/10.1016/j.celrep.2015.12.018

SUMMARY

Subtype-specific neurons obtained from adult humans will be critical to modeling neurodegenerative diseases, such as amyotrophic lateral sclerosis (ALS). Here, we show that adult human skin fibroblasts can be directly and efficiently converted into highly pure motor neurons without passing through an induced pluripotent stem cell stage. These adult human induced motor neurons (hiMNs) exhibit the cytological and electrophysiological features of spinal motor neurons and form functional neuromuscular junctions (NMJs) with skeletal muscles. Importantly, hiMNs converted from ALS patient fibroblasts show disease-specific degeneration manifested through poor survival, soma shrinkage, hypoactivity, and an inability to form NMJs. A chemical screen revealed that the degenerative features of ALS hiMNs can be remarkably rescued by the small molecule kenpaullone. Taken together, our results define a direct and efficient strategy to obtain disease-relevant neuronal subtypes from adult human patients and reveal their promising value in disease modeling and drug identification.

INTRODUCTION

Amyotrophic lateral sclerosis (ALS), also known as Lou Gehrig's disease, is a devastating adult-onset neurological disorder prevalent worldwide with no effective cure (Arbab et al., 2014; Gladman et al., 2012). ALS is characterized by progressive motor neuron (MN) dysfunction and death; however, the mechanisms leading to selective MN loss around the age of onset remain poorly understood (Arbab et al., 2014; Robberecht and Philips, 2013). This is largely due to the lack of available patient-specific MNs during disease progression (Arbab et al., 2014). Studies of post-mortem tissues, as well as transgenic cellular and animal models, have provided valuable insights into pathogenic ALS phenotypes (Bruijn et al., 1998; Gurney et al., 1994; Hadzipasic et al., 2014; Haidet-Phillips et al., 2011; Kiernan and Hudson, 1991; Qiu et al., 2014; Re et al., 2014; Spalloni et al., 2011; Wada et al., 2012). Nonetheless, major discrepancies and controversies exist in these models owing to genetic, anatomical, and experimental variations (Bories et al., 2007; Delestrée et al., 2014; Haidet-Phillips et al., 2011; Kuo et al., 2004; Leroy et al., 2014; Re et al., 2014; Saxena et al., 2013). Unsurprisingly, no therapeutic has succeeded in translation to the clinic (Gladman et al., 2012; Musarò, 2013).

Induced pluripotent stem cells (iPSCs) derived from human skin fibroblasts and differentiated into spinal MNs are emerging as a cellular model for investigating ALS (Chen et al., 2014; Dimos et al., 2008; Kiskinis et al., 2014). This model utilizes genetic mutation(s) naturally occurring in human patients and thus avoids potential pitfalls associated with ectopic overexpression of mutant genes. New insights into the pathology of ALS have been gained with this model (Chen et al., 2014; Kiskinis et al., 2014); however, the generation of iPSCs and their stepwise differentiation into MNs are lengthy and complex processes accompanied by technical limitations due to iPSC line variation and the heterogeneity of differentiated neurons (Arbab et al., 2014). Furthermore, because iPSCs are reset to an embryonic stage during reprogramming (Lapasset et al., 2011; Miller et al., 2013; Rando and Chang, 2012), a major difficulty with modeling ALS is the induction of an adult-onset pathology using iPSC-derived fetal stage neurons (Arbab et al., 2014).

Direct lineage reprogramming bypasses pluripotency and converts fully differentiated somatic cells into functional neurons (Pang et al., 2011; Vierbuchen et al., 2010; Yoo et al., 2011). This technology is also capable of creating subtype-specific neurons, such as dopaminergic neurons (Caiazzo et al., 2011), striatal medium spiny neurons (Victor et al., 2014), nociceptive neurons (Wainger et al., 2015), and cholinergic neurons (Liu et al., 2013; Son et al., 2011). Despite limitations with reprogramming efficiency and neuronal purity, directly converted subtype-specific neurons are potentially more valuable to disease modeling and drug identification for late-onset human neurological disorders (Arbab et al., 2014). As a proof-of-concept study, we provide a protocol for direct and highly efficient conversion of adult human fibroblasts to functionally mature MNs with high purity. We further reveal pathology of MNs derived from ALS patient fibroblasts with FUS mutations. Most importantly, a pilot drug screen

identified a small molecule capable of rescuing key deficits in these diseased MNs.

RESULTS

Rapid and Efficient Conversion of Adult Human Fibroblasts to MNs

We previously demonstrated that postnatal and adult human fibroblasts can be rapidly and efficiently converted to (human induced) cholinergic neurons (hiCNs) through the synergistic actions of extrinsic and intrinsic cues (Liu et al., 2013). However, these hiCNs lack the expression of ISL1 and LHX3, two factors essential to the development of MNs (Thaler et al., 2002). We then examined whether hiCNs can be further specified to a bona fide MN fate. cDNAs encoding ISL1 and LHX3 were subcloned into a polycistronic lentiviral vector for expression at a 1:1 ratio, as this is essential for MN specification (Lee et al., 2012). Primary fibroblasts (Table S1) from three normal (NL) healthy adult humans (AG05811, 71 years, designated NL1; AG07473, 50 years, designated NL2; and AG09969, 53 years, designated NL3) were co-transduced with lentiviruses expressing NEUROG2-IRES-GFP-T2A-SOX11 and ISL1-T2A-LHX3 (hereafter referred to as NSIL). Then, 2 days post-viral infection (dpi), these cells were switched to neuron-induction media containing our previously identified extrinsic factors, forskolin (FSK) and dorsomorphin (DM), and basic fibroblast growth factor (FGF2) (Liu et al., 2013). Neuronal conversion was monitored daily by live-cell fluorescence microscopy and analyzed by immunocytochemistry at the indicated time points.

Remarkably, 86%–96% of NSIL virus-transduced adult fibroblasts (indicated by GFP co-expression) were converted to TUBB3$^+$ neuron-like cells by 14 dpi (Figures 1A and 1B). During this conversion process, cells rapidly changed their initially flat, spread-out morphology to one with bipolar and multipolar processes. They progressively became more elaborate with round or pyramidal somas, condensed nuclei, long axons, and multiple neurites, as indicated by specific staining with the pan-neuronal markers MAP2 and NF200 at 21 dpi (Figures 1C and 1D). The converted cells also expressed the presynaptic marker synaptotagmin 1 (SYT1) in a discrete punctate pattern, suggesting the establishment of synaptic terminals by 21 dpi in culture (Figure 1E). The inclusion of FSK, DM, and FGF2 in the culture media is essential for efficient neuronal reprogramming, as omission of any small molecule or FGF2 greatly reduced the population of TUBB3$^+$ cells (Figures S1A and S1B).

Immunocytochemistry showed that the reprogrammed neurons exclusively expressed markers for spinal MNs, including HB9, CHAT, and VACHT (Figures 1A and 1F–1I). Over 84% and 95% of TUBB3$^+$ cells co-stained with HB9 and CHAT, respectively. In sharp contrast, none expressed markers for dopaminergic (TH) or GABAergic (GAD67) neurons. These data indicate that adult human fibroblasts are reprogrammed into spinal (human induced) MNs (hiMNs). Our qRT-PCR analysis of *HOX* gene expression showed that hiMNs are a mixture of cervical and/or thoracic spinal MNs (Figure S1C).

When co-cultured with mouse astrocytes, hiMNs survived over 49 dpi, outgrew multiple long processes, and formed dense neuronal networks throughout the whole culture (Figure 1J). Compared to cells at earlier stages (Figures 1A and 1H), the expression of HB9 was much reduced or diminished by 49 dpi (Figure 1K), resembling its endogenous expression pattern in more mature spinal MNs (Detmer et al., 2008). In contrast, hiMNs maintained strong CHAT expression, indicative of cholinergic neurotransmitter synthesis (Figure 1K).

Direct Fate Switch without a Progenitor Stage

A time course analysis showed that around 46% and 90% of the virus-transduced cells expressed the mature neuronal marker MAP2 at 7 and 10 dpi, respectively (Figure S1D). During this process, proliferative neural progenitors were not involved in the NSIL-mediated conversion of adult human fibroblasts. Cell proliferation was examined by 2-hr pulse labeling with 5-bromodeoxyuridine (BrdU) before immunocytochemical analyses at 0, 1, 3, 7, and 10 dpi, respectively (Figures S1D and S1E). The non-transduced control cells were efficiently BrdU labeled under this condition. However, none of the converted MAP2$^+$ cells incorporated BrdU when pulsed at 7 or 10 dpi (Figures S1D and S1E). BrdU incorporation appeared to be nontoxic to converted neurons, as a majority could be labeled by BrdU if the proliferating fibroblasts were initially treated with BrdU 2 hr before lentiviral infection (Figures S1D and S1E). The neural progenitor markers SOX2 and OLIG2 were never detected during the early reprogramming process (Figure S1F). As controls, SOX2 and OLIG2 also failed to induce any neuronal conversion of human fibroblasts. Together, these data indicate that adult human fibroblasts are directly and efficiently reprogrammed to highly pure hiMNs under a defined culture condition.

Functional Maturation of hiMNs

The electrophysiological properties of hiMNs were determined by whole-cell patch-clamp recordings. All the recorded hiMNs reprogrammed from normal adult human fibroblasts fired repetitive action potentials (APs) upon current injection when examined at 49 dpi or beyond (Figure 2A). In voltage-clamp mode, hiMNs showed tetrodotoxin (TTX)-sensitive inward currents, indicating sodium current influx through voltage-gated sodium channels (Figures 2B and 2C). These channels have stereotypical fast activation and slow inactivation characteristics (Figures 2C and 2D). The hiMNs converted from all healthy human patient fibroblasts exhibited similar excitability, including AP firing threshold, frequency, half-width, amplitude, and the delay of the first spike (Figures 2E–2I). There were also no major differences in channel properties among these hiMNs, as measured approximately by sodium and potassium current amplitudes (Figures 2J–2L and S2). GABA, glycine, and glutamate receptors on hiMNs could be activated by puffs of their respective agonists. This illustrates the presence of both functional inhibitory and excitatory postsynaptic receptors on reprogrammed hiMNs (Figure 2M). Robust spontaneous postsynaptic currents (sPSCs) could be detected when hiMNs were co-cultured with mouse cortical neurons, indicating functional synapse formation between these neuron populations (Figure 2N; n = 23; 0.266 ± 0.104 Hz and 13.034 ± 3.522 pA for average frequency and amplitude, respectively). Together, these data demonstrate that hiMNs become electrophysiologically mature.

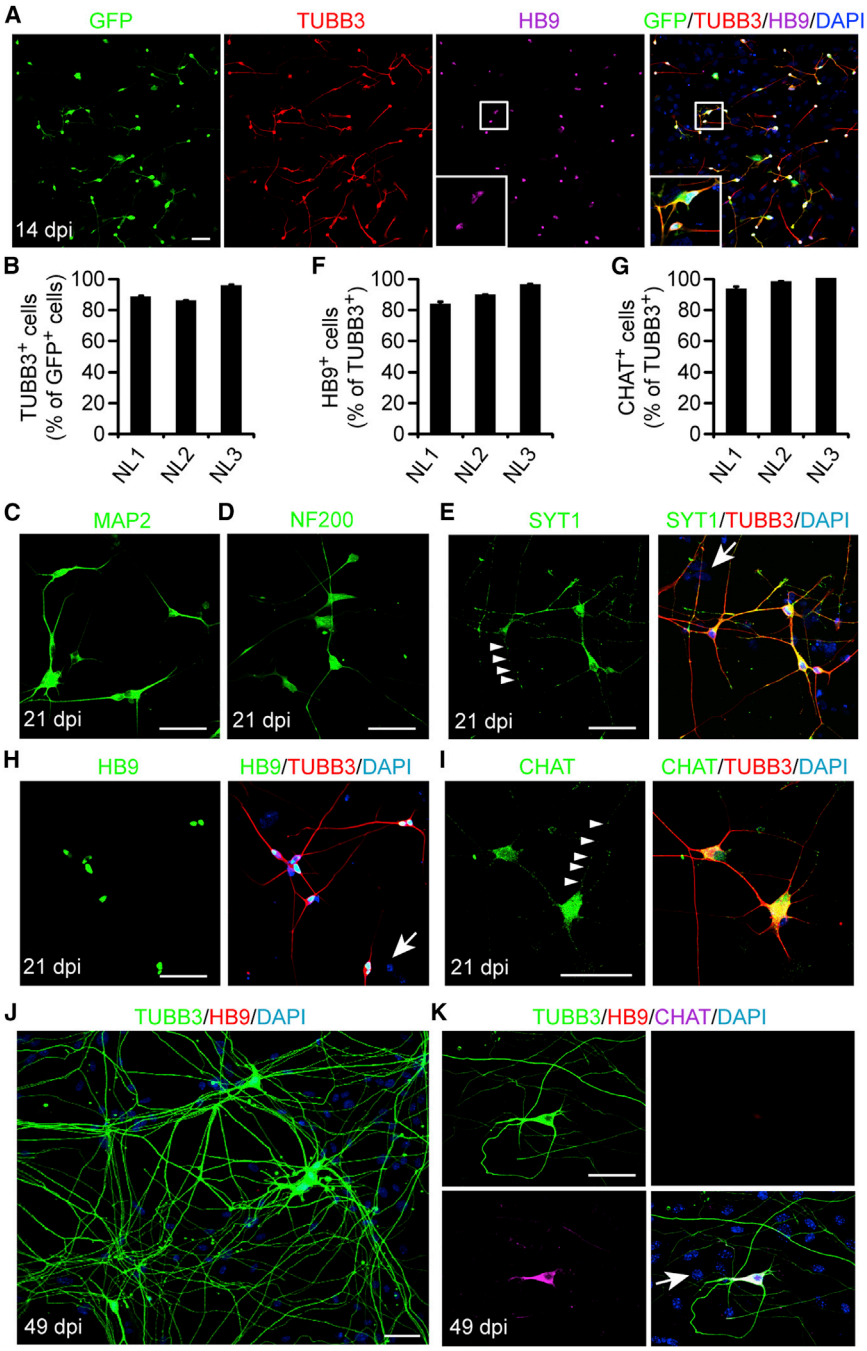

Figure 1. Rapid and Efficient Conversion of Adult Human Fibroblasts to hiMNs

(A) Neuronal marker expression in adult human fibroblast (NL1)-derived hiMNs at 14 days post-infection (dpi). The virus-transduced cells are indicated by GFP fluorescence. Scale bar, 50 μm.

(B) Reprogramming efficiency determined by TUBB3 expression at 14 dpi is shown (mean ± SEM, n = 3 independent samples, 20 randomly selected 20× fields per sample were examined).

(C–E) Immunofluorescent visualization of the indicated markers in hiMNs at 21 dpi. The punctate-staining pattern of SYT1 in neuronal processes is indicated by the arrowheads, while the arrow indicates a non-converted cell within the same image field. Scale bars, 50 μm.

(F and G) Neuronal purity was determined by the expression of MN markers at 21 dpi (mean ± SEM, n = 3 independent samples with ≥600 cells in each group).

(H and I) Immunofluorescent visualization of marker expression for hiMNs at 21 dpi. The punctate-staining pattern of CHAT in neuronal processes is indicated by the arrowheads, while the arrow indicates a non-converted cell within the same image field. Scale bars, 50 μm.

(J and K) hiMN morphology and marker expression at 49 dpi. HB9 expression is significantly reduced in more mature hiMNs while robust CHAT expression persists. A marker-negative cell is indicated by an arrow. Scale bars, 50 μm.

See also Figure S1 and Table S1.

A key feature of spinal MNs is their ability to form functional neuromuscular junctions (NMJs). This was determined through co-culture of hiMNs and primary mouse skeletal myotubes. Extensive growth and branching of hiMN axons were observed 3–7 days after co-culture (Figures 3A and 3B). Many axons projected along multinucleated myotubes, which stained positive for the mature muscle marker myosin heavy chain (MHC). At sites of contact with myotubes, the enlarged presynaptic SYN$^+$ axonal terminals of hiMNs frequently aligned with the clustered postsynaptic acetylcholine receptors, which were specifically detected by rhodamine-labeled α-bungarotoxin (α-BTX) on the muscle surface (Figure 3B). As controls, acetylcholine receptor clustering was not observed on myotubes when cultured alone or with primary mouse cortical neurons (Figures 3C and 3D). These data suggest that mature hiMNs uniquely induce the formation of NMJs with cultured muscles.

Whole-cell patch-clamp recordings were then performed on co-cultured myotubes to determine whether these newly formed NMJs were functional (Figure 3E). Robust spontaneous end plate currents (sEPCs) were detected from myotubes co-cultured with hiMNs, but not from those cultured alone or with cortical neurons (Figures 3F, S3A, and S3B). These currents could be specifically blocked by wash-in of the acetylcholine receptor antagonist (+)-tubocurarine during recordings (Figures 3G, S3C, and S3D). This confirmed that the observed sEPCs were mediated by established NMJs. Larger sEPCs also could be eliminated by blocking neuron-specific voltage-gated sodium channels with TTX (Figures 3H, S3C, and S3D). Interestingly, smaller sEPCs could still be observed under this condition, reflecting TTX-insensitive quantum release of synaptic vesicles from hiMNs to the co-cultured muscles. In contrast, sEPCs were not

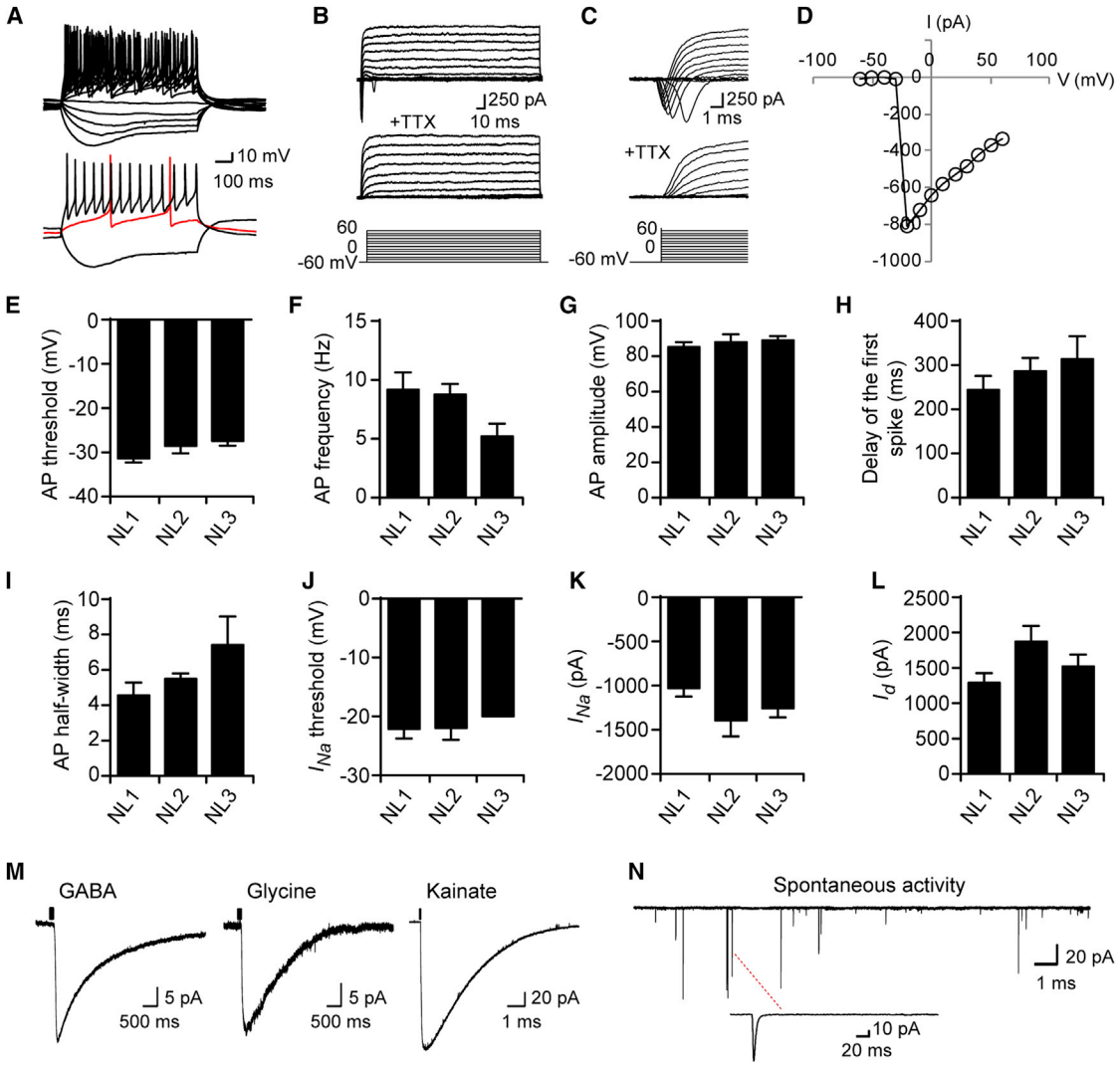

Figure 2. Electrophysiological Properties of hiMNs

(A) Repetitive AP waveforms recorded under current-clamp mode. The precondition sweep and sweeps immediately above threshold and at the highest frequency are shown in the lower panel.

(B) Representative potassium and TTX-sensitive sodium currents are shown.

(C) A zoomed-in view of TTX-sensitive sodium currents presented in (B) is shown.

(D) A plot of the sodium current (I)-voltage (V) curve is shown.

(E–L) Control hiMNs exhibit comparable electrophysiological properties (mean ± SEM; NL1, n = 21; NL2, n = 7; NL3, n = 6).

(M) Representative electrophysiological responses of hiMNs to puffs of receptor agonists are shown (n = 3 for GABA, n = 2 for glycine, and n = 4 for kainate).

(N) Representative traces of spontaneous postsynaptic currents (sPSCs) recorded from hiMNs are shown.

See also Figure S2 and Table S2.

significantly altered when muscle-specific voltage-gated sodium channels were inhibited by the antagonist μ-connotoxin (Figures 3I, S3C, and S3D). Together, these data reveal that hiMNs functionally innervate co-cultured skeletal muscles and control their activities through the NMJ formations.

Efficient Conversion of ALS Patient Fibroblasts to hiMNs

We applied the same reprogramming process to skin fibroblasts derived from three ALS patients aged between 37 and 50 years (Table S1). These patients were identified to harbor genetic mutations in the *FUS* gene, including a synonymous mutation (c.1566G > A) that does not change the FUS amino acid sequence (ND29563, 37 years, mutation R522R, designated ALS1) (Lai et al., 2011); a mutation that alters protein sequence but has no clear effect on protein subcellular localization (ND39027, 50 years, mutation H517Q, designated ALS2) (Kwiatkowski et al., 2009); and a mutation that alters amino acid sequence, resulting in FUS cytoplasmic translocation (ND40077, 47 years, mutation R521G, designated ALS3) (Kwiatkowski et al., 2009). ALS patient-derived fibroblasts could be efficiently reprogrammed into

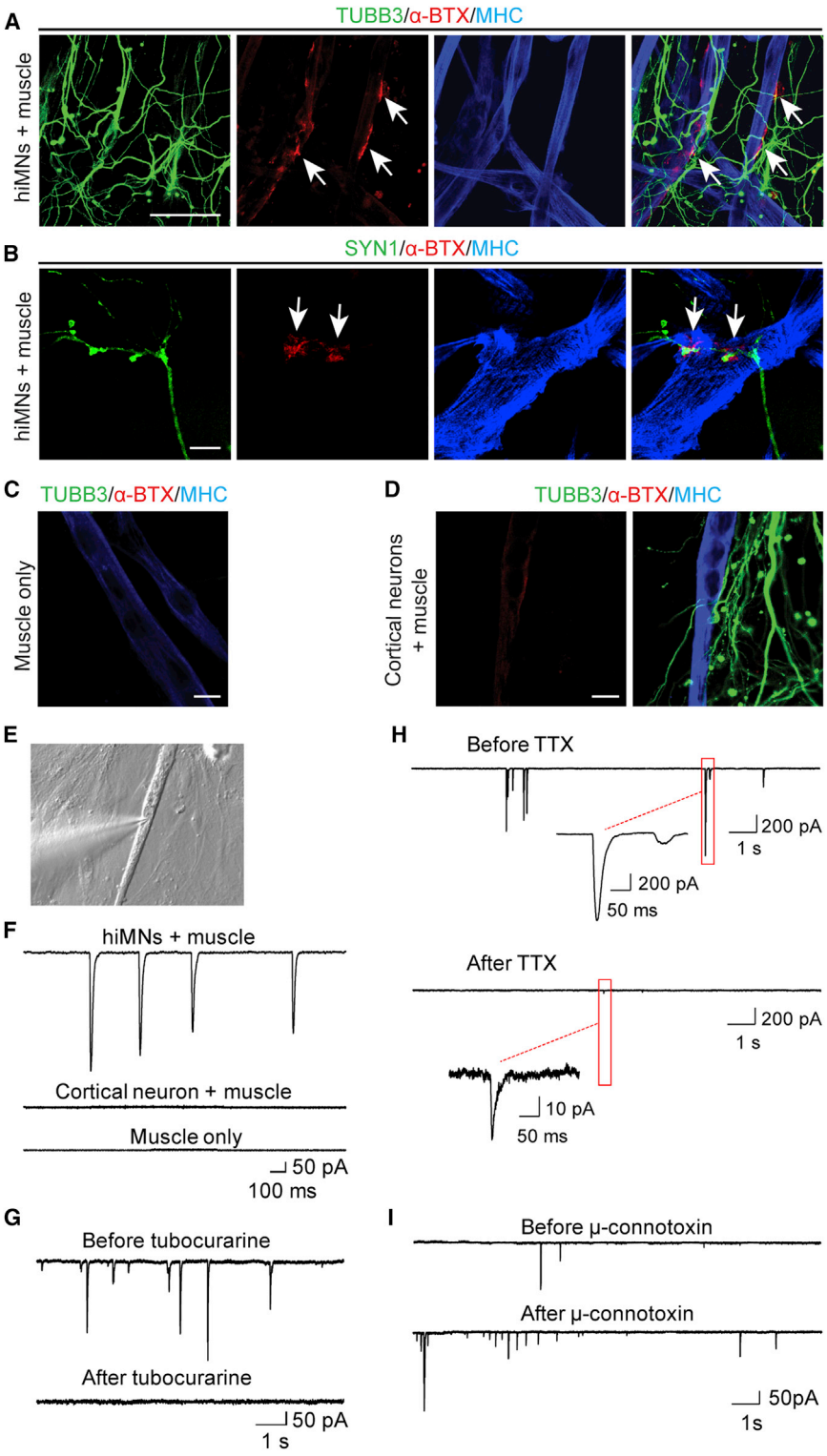

Figure 3. hiMNs Induce Functional NMJs

(A and B) Immunofluorescent visualization of typical neuromuscular junctions (NMJs, indicated by arrows) that formed between hiMNs and primary mouse myotubes in co-culture are shown. Scale bars, 50 (A) and 10 μm (B).

(C and D) NMJs were not detectable when myotubes were cultured alone (C) or with cortical neurons (D). Scale bars, 10 μm.

(E) A typical image shows a glass pipette-patched myotube in culture.

(F) Spontaneous end plate currents (sEPCs) were detected in myotubes when co-cultured with hiMNs (n = 36), but not when cultured alone (n = 9) or with cortical neurons (n = 13).

(G) sEPCs are sensitive to the acetylcholine receptor antagonist (+)-tubocurarine (n = 4).

(H) sEPCs are sensitive to treatment with tetrodotoxin (TTX), a specific inhibitor of voltage-gated sodium channels in neurons (n = 6). Miniature TTX-insensitive currents were still detectable.

(I) sEPCs are insensitive to treatment with μ-connotoxin, a specific inhibitor of voltage-dependent sodium channels in muscles (n = 3).

See also Figure S3.

neurons with 80%–93% of surviving NSIL-transduced cells expressing TUBB3 by 14 dpi (Figures 4A and 4B). The converted cells also expressed the pan-neuronal markers MAP2 and NF200, as well as the presynaptic marker SYT1, by 21 dpi (Figures 4C–4E). These cells displayed typical MN morphology with multiple dendrites and prominent axon. Immunocytochemistry further revealed that 84%–87% and 95%–97% of TUBB3$^+$ cells co-stained for HB9 and CHAT, respectively (Figures 4F–4I). Together, these data demonstrate that fibroblasts derived from adult ALS patients can be efficiently converted to highly pure hiMNs, hereby referred to as ALS hiMNs. These data also indicate that *FUS* mutations do not impede neuronal reprogramming of adult patient fibroblasts, which is consistent with the fact that neuronal development is not obviously altered in these patients.

Mislocalization of FUS in ALS hiMNs

Cytoplasmic retention of the mutated FUS protein is a major pathological feature identified in spinal MNs of ALS patients (Kwiatkowski et al., 2009; Vance et al., 2009). As such, we examined the expression and subcellular localization of FUS protein in fibroblasts and hiMNs. Western blot analysis did not reveal any significant difference on the level of endogenous FUS in fibroblasts obtained from both ALS patients and healthy controls (Figure 5A). Immunocytochemistry showed a predominant nuclear distribution of endogenous FUS but failed to detect a major difference between these fibroblast lines (Figure 5B). In sharp contrast, the subcellular distribution of FUS protein was

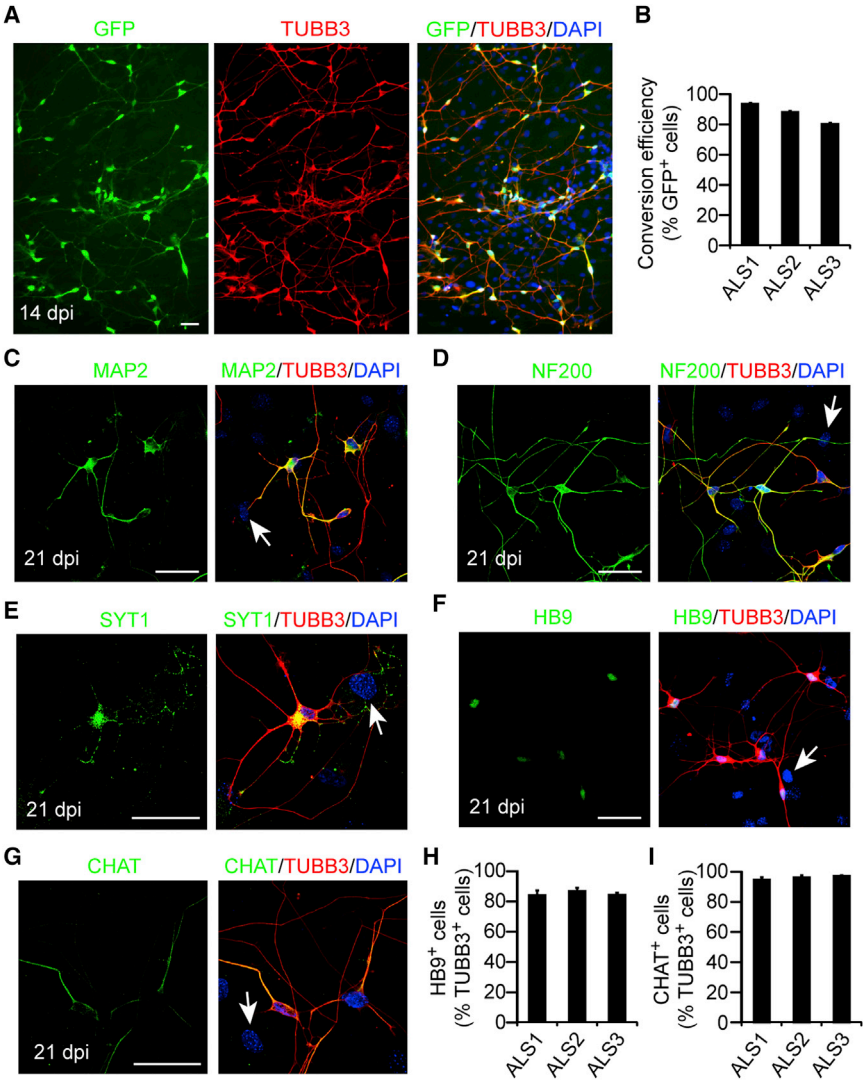

Figure 4. hiMNs Converted from Fibroblasts of Adult Human ALS Patients

(A) Neuronal conversion of fibroblasts from human ALS patients. Virus-transduced cells are indicated by GFP fluorescence. Scale bar, 50 μm.

(B) Conversion efficiency as determined by TUBB3 expression at 14 dpi is shown (mean ± SEM, n = 3 independent samples, 20 randomly selected 20× fields per sample were examined).

(C–E) Immunofluorescent visualization of neuronal marker expression in converted cells from ALS patients. Arrows show marker-negative cells. Scale bars, 50 μm.

(F and G) Reprogrammed neurons from ALS patients express markers for spinal MNs. Arrows show marker-negative cells. Scale bars, 50 μm.

(H and I) Neuronal purity was determined by expression of MN markers at 21 dpi (mean ± SEM, n = 3 independent samples with ≥600 cells counted for each group).

See also Table S1.

significantly different when these fibroblasts were converted to hiMNs. Compared to normal controls, a larger fraction of endogenous FUS was mislocated into the cytoplasm of ALS hiMNs (Figures 5C and 5D), consistent with post-mortem analysis of spinal MNs from ALS patients with mutant FUS (Kwiatkowski et al., 2009; Vance et al., 2009).

Given that amino acid sequence is not altered in the synonymous c.1566G > A *FUS* mutant (ALS1 patient), its mislocalization was somewhat unexpected; however, it may not be totally surprising. A synonymous mutation in the multidrug resistance 1 (MDR1) gene was shown to affect the timing of co-translational folding and, therefore, to alter the structure of substrate and inhibitor interaction sites (Kimchi-Sarfaty et al., 2007). Recent studies also confirmed that synonymous codons have a huge influence on the rate of translation elongation and subsequent protein folding, structure, and function (Yu et al., 2015; Zhou et al., 2013, 2015). Although systematic studies are required to determine how synonymous c.1566G > A mutation leads to the mislocalization of FUS protein, it is highly possible that this mutation results in altered protein folding and structure. Of note, the c.1566G > A variant frequently was associated with ALS patients (Lai et al., 2011), although it also was detected in certain control samples (Corrado et al., 2010). It would be interesting to determine whether the control samples with this synonymous mutation eventually develop ALS at a later stage. Notwithstanding, other genetic and non-genetic causes are not excluded for ALS patients with synonymous FUS mutations. The ALS1 patient may well represent a sporadic case.

Morphological and Survival Deficits of ALS hiMNs

A hallmark of ALS is the progressive degeneration and loss of MNs (Cleveland and Rothstein, 2001; Pasinelli and Brown, 2006). We examined cell morphology and survival of hiMNs co-cultured with wild-type mouse astrocytes. ALS hiMNs exhibited shrunken somas with sizes ranging from 198 to 247 μm^2 at 49 dpi. This is significantly smaller than hiMNs derived from age-matched healthy controls, which had soma sizes ranging from 292 to 330 μm^2 (Figures 6A–6C). Shrinkage of spinal MN somas has been observed in post-mortem human ALS patients and is believed to precede neuronal death (Kiernan and Hudson, 1991).

In contrast to the similar survival rates among all normal hiMNs, ALS hiMNs were more susceptible to death with survival rates of 45%–65%, 9%–48%, and 8%–37% relative to normal hiMNs when examined at 21, 35, and 49 dpi, respectively (Figure 6D). To ascertain whether these survival deficits can be caused by mutations in FUS, we transduced normal healthy fibroblasts (NL1) with virus expressing ALS patient-specific FUS mutants. These ectopic mutant proteins either have a predominant nuclear localization similar to wild-type FUS (H517Q) or are diffusedly localized in the cell (R514G, R521C, and R522G;

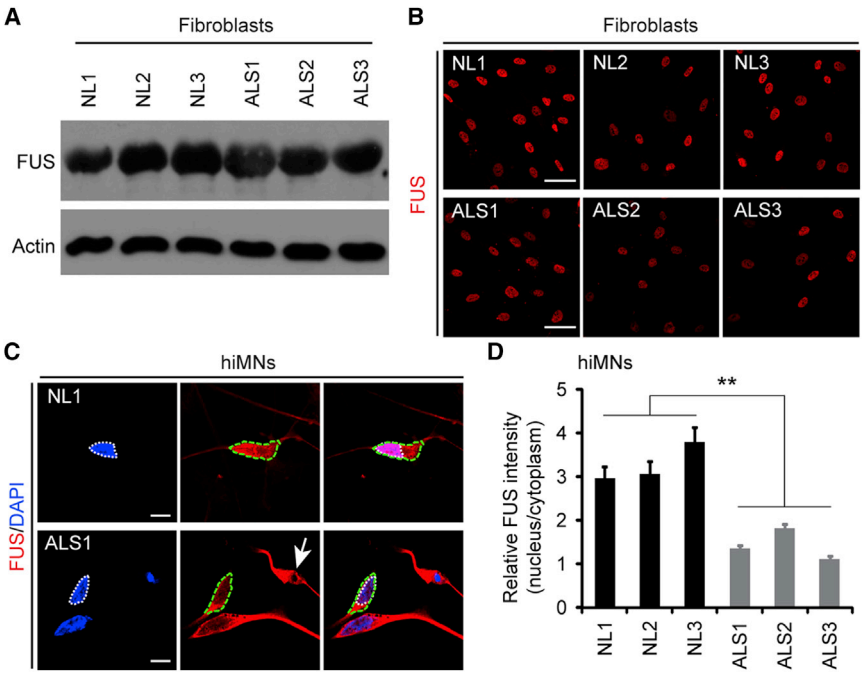

Figure 5. Mislocalization of FUS in ALS hiMNs

(A) Western blot analysis of FUS expression in fibroblasts is shown.

(B) Confocal images show subcellular distribution of FUS in fibroblasts. Scale bars, 50 μm.

(C) Expression and distribution of FUS in hiMNs. The nucleus and soma are outlined with white and green lines, respectively. The arrow indicates complete nuclear exclusion of FUS in some dying ALS1 hiMNs. Scale bars, 10 μm.

(D) Quantification of subcellular FUS distribution in hiMNs (mean ± SEM, n = 50 cells from three independent samples for each group, **p = 0.005).

Figure S4A). Western blot analysis showed a comparable expression of ectopic and endogenous FUS (Figures S4B and S4C). Compared to normal healthy cells transduced with either an empty or wild-type *FUS* virus, hiMNs converted from *FUS* mutant virus-transduced normal fibroblasts showed a significant reduction in survival when examined at 21 dpi (Figure 6E), recapitulating the deficits observed in ALS hiMNs. Together, the morphological and survival deficits of ALS hiMNs match those pathological phenotypes detected in post-mortem tissues (Kiernan and Hudson, 1991), animal ALS models (Hadzipasic et al., 2014; Qiu et al., 2014), and iPSC-derived MN models (Kiskinis et al., 2014).

Electrophysiological Deficits of ALS hiMNs

The electrophysiological properties of ALS hiMNs derived from ALS1 and ALS2 patients were examined in detail at 49 dpi and beyond. ALS1 and ALS2 hiMNs were representative of the survival extremes among reprogrammed ALS hiMNs (Figure 6D). Whole-cell patch-clamp recordings showed that ALS hiMNs, similar to normal controls, exhibited typical inward sodium currents and outward potassium currents (Figures S5A–S5C), suggesting that they acquired basic neuronal properties. The amplitudes of sodium and potassium currents were comparable, although the normalized values by membrane capacitance were much reduced for ALS hiMNs (Figures S5D and S5E). Most interestingly, ALS hiMNs showed dramatic deficits in AP firing (Figure 6F). Unlike control hiMNs that could fire repetitive APs at later culture time points, the ALS hiMNs fired very infrequently at all the time points examined (Figure S5F). Statistical analyses showed that the threshold, frequency, amplitude, and half-width of APs, as well as delay of the first spike, were significantly different between normal and ALS hiMNs (Figures 6G–6K).

Furthermore, synaptic connectivity was investigated in co-culture. When acting as the postsynaptic neuron in co-culture with mouse cortical neurons, normal and ALS hiMNs showed comparable sPSC frequency and amplitude, suggesting that ALS hiMNs formed normal synapses with presynaptic neurons and received inputs from these cells (Figures 6L–6N). The presynaptic functionality of ALS hiMNs and NMJ formation were examined in co-culture with primary mouse skeletal muscles. Compared to normal hiMNs, ALS hiMNs rarely induced NMJ formation (Figures 6O and 6P). Consistent with this morphological deficit, whole-cell patch-clamp recordings performed on muscles showed that sEPCs were not or rarely detected when co-cultured with ALS hiMNs, revealing profound dysfunction in the ability of these diseased MNs to control muscle contraction (Figures 6Q–6S).

A Screen of Small Molecules Aiming to Promote ALS hiMN Survival

We observed that hiMNs are sensitive to systemic stress induced by a replating procedure during culture. Over 80% of ALS1 hiMNs died 3 days post-replating on matrigel/laminin-coated culture vessels at 14 dpi (Figure S6A). Co-culture with primary mouse astrocytes also led to over 60% death of these cells 7 days after replating. Using this stress-accelerated cell death model, we performed a pilot screen of small molecules that promote the survival of ALS hiMNs. These candidates included valproic acid (VPA) (Leng et al., 2008; Niu et al., 2013), isoxazole (ISX) (Ryan et al., 2013), lithium chloride (LiCl) (Leng et al., 2008), kenpaullone (Ken) (Yang et al., 2013), and an aminopropyl carbazole derivative (P7C3) (Pieper et al., 2010), which are known to promote neuronal survival. Consistently, the survival of ALS1 hiMNs on matrigel/laminin-coated plates was enhanced by each of these candidate molecules at an appropriate concentration, though the effect of Ken was modestly superior (Figure S6B). We then reexamined these molecules on ALS1 hiMNs that were replated on astrocyte-coated plates. Interestingly, Ken was the most effective at promoting the survival of these cells, while the remaining chemicals were not as effective under this culture condition (Figure S6C). A binary combination of these chemicals did not outperform Ken alone. A dosage analysis

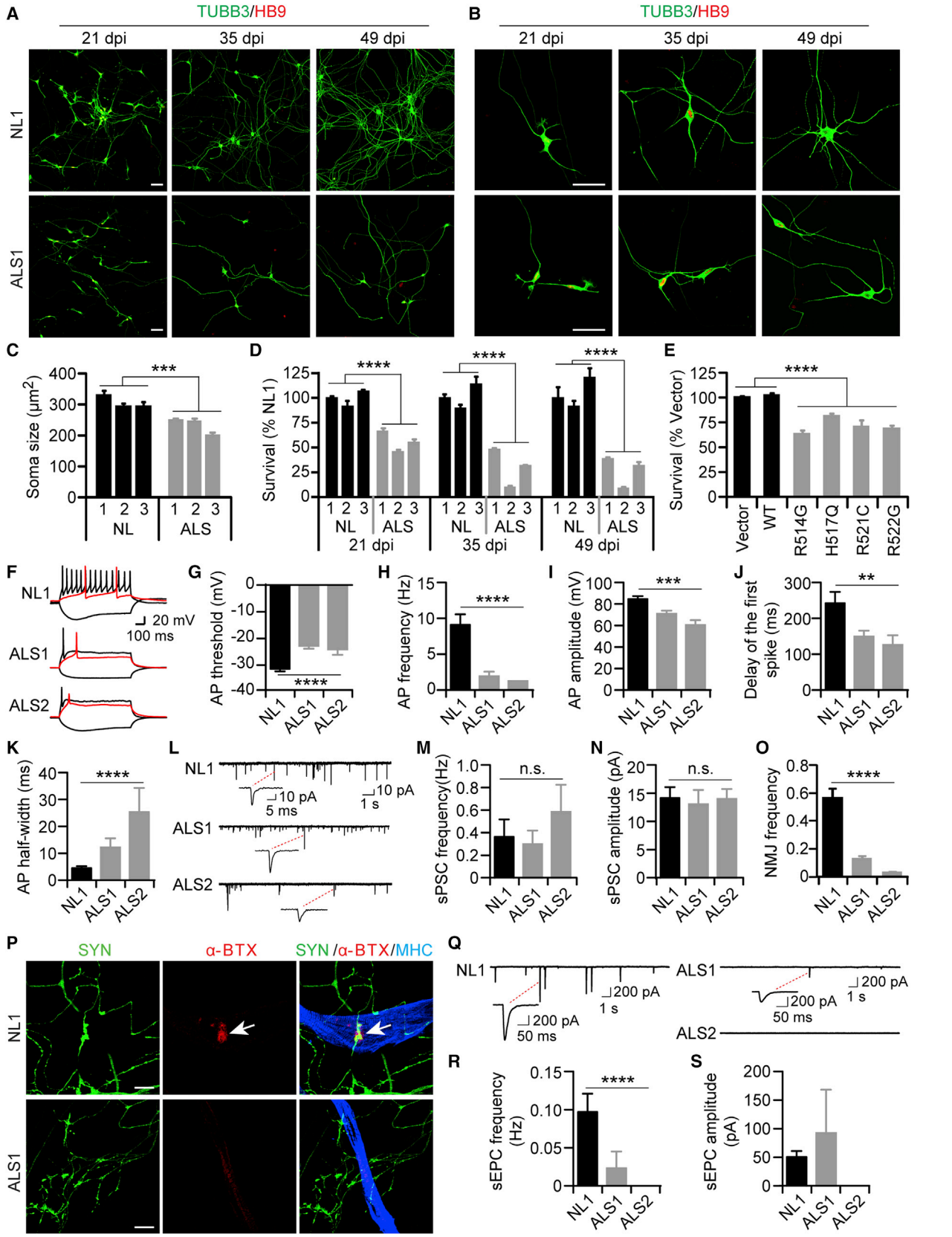

(legend on next page)

showed that the optimal concentration for Ken was 1 μM, while concentrations higher than 5 μM can result in chemical precipitation and loss of the protective effect (Figures S6D and S6E).

Functional Rescue of ALS hiMNs by Ken

The effect of Ken was further evaluated on ALS hiMNs derived from all three FUS patients and co-cultured with astrocytes. Compared to vehicle controls, Ken greatly enhanced the outgrowth and branching of neuronal processes at all the time points examined (Figures 7A and 7B). Ken-treated ALS hiMNs formed a super-dense neuronal network more evident at 35 dpi and thereafter (Figure 7A). These cells also had larger somas, which were quantified by measuring randomly chosen cells from triplicate experiments (Figure 7C). There was an average 1.43- to 1.94-fold increase of soma size for Ken-treated ALS hiMNs when compared to their respective vehicle-treated controls at 49 dpi. A time course analysis revealed a remarkable long-term effect of Ken on cell survival, with 2.4–4.7 times more Ken-treated cells surviving relative to vehicle controls when examined at 49 dpi (Figure 7D). Ken treatment also enabled hiMNs to survive for months on matrigel/laminin-coated dishes. These cells formed massive SYN1$^+$/TUBB3$^+$ neuronal networks (Figure S6F). Together, these data clearly indicate that the morphological and survival deficits of ALS hiMNs are greatly improved by the small molecule Ken.

We then determined whether Ken treatment also ameliorated the profound electrophysiological defects shown by ALS hiMNs (Figures 6F–6S). Normal and ALS hiMNs were treated with Ken starting at 14 dpi and examined by whole-cell patch-clamp recordings at 49 dpi or later. Compared to vehicle-treated ALS hiMNs, which were hypoactive and rarely exhibited multiple APs (Figure 6F), Ken-treated ALS hiMNs fired repetitively in a manner similar to control hiMNs, suggesting the restoration of normal excitability (Figure 7E). Statistical quantification revealed a remarkable rescue of ALS hiMNs by Ken in all aspects of electrophysiological properties, including AP threshold, frequency, amplitude, and half-width, as well as the delay of the first spike (Figures 7F–7J and S7).

Postsynaptic activities were examined by co-culturing hiMNs with primary mouse cortical neurons. Robust sPSCs were detected in all Ken-treated hiMNs and no significant difference was observed in either frequency or amplitude (Figures 7K–7M). Interestingly, sPSCs often occurred in bursts, suggesting activation of hiMNs by a more active neuronal network and strong synaptic connectivity between hiMNs and the co-cultured cortical neurons. Presynaptic function of hiMNs was examined through co-culture with primary mouse skeletal muscles. In sharp contrast to the dysfunction of vehicle-treated ALS hiMNs to innervate muscles (Figures 6O and 6P), Ken treatment enabled these hiMNs to induce NMJs with a comparable frequency to that of normal hiMNs (Figures 7N and 7O). Patch-clamp recordings on myotubes co-cultured with ALS hiMNs showed similar sEPCs as those co-cultured with the normal healthy hiMNs (Figures 7P–7R). Taken together, these data demonstrate that Ken treatment is able to robustly rescue ALS hiMN dysfunction.

DISCUSSION

Analysis of human post-mortem tissues reveals that the degeneration and death of MNs are the pathological basis for human ALS (Kwiatkowski et al., 2009; Vance et al., 2009). However, one paramount challenge studying this neurodegenerative disease is the lack of a model system for human patient-specific MNs. As such, transgenic cellular and animal models traditionally have been employed (Bruijn et al., 1998; Gurney et al., 1994; Howland et al., 2002; Qiu et al., 2014; Rosen, 1993; Sreedharan et al., 2008; Wada et al., 2012). Although important insights into the pathogenesis of ALS were garnered, the genetic and anatomical differences between these models and human patient MNs inevitably raised critical concerns as to artifacts intrinsically associated with these non-natural transgenic models (Bergemalm et al., 2006; Julien and Kriz, 2006; Kiskinis et al., 2014). A recent cellular model with iPSC-derived MNs overcame many of these concerns, as these cells inherited all the natural genetic variations linked to ALS pathology (Arbab et al., 2014; Chen et al., 2014; Dimos et al., 2008; Kiskinis et al., 2014). Nevertheless, iPSC-differentiated neurons remain at an embryonic stage (Lapasset et al., 2011; Miller et al., 2013; Rando and Chang, 2012), and it is uncertain whether the defects identified

Figure 6. Pathophysiology of ALS hiMNs

(A and B) Representative morphology of hiMNs derived from both normal and FUS patients at the indicated time points in culture. Images in (B) are higher magnification views of hiMNs. Scale bars, 50 μm.

(C) Soma size was measured at 49 dpi (mean ± SEM, n = 3 independent samples with ≥150 neurons analyzed for each group, ***p < 0.001).

(D) Poor survival of ALS hiMNs at the indicated time points is shown (mean ± SEM, n = 3 independent samples for each group, ****p < 0.0001).

(E) Reduced survival of hiMNs converted from normal fibroblasts (NL1) with ectopic expression of the indicated FUS mutants. Cells were counted at 21 dpi (mean ± SEM, n = 3 independent samples for each group, ****p < 0.0001).

(F) Representative AP waveforms for the indicated samples. Red and black traces represent the AP immediately above threshold and firing at the highest frequency, respectively.

(G–K) Electrophysiological deficits of ALS hiMNs are shown (mean ± SEM; NL1, n = 21; ALS1, n = 28; ALS2, n = 8; **p < 0.01, ***p < 0.001, and ****p < 0.0001).

(L) Representative traces of sPSCs recorded from hiMNs co-cultured with cortical neurons are shown.

(M and N) Quantification of sPSC frequency and amplitude. No significant differences were found between the indicated samples (mean ± SEM; NL1, n = 17; ALS1, n = 16; and ALS2, n = 5; n.s., not significant).

(O) Quantification of NMJ frequency is shown (mean ± SEM, n = 3 independent samples with 300 hiMN network-associated myotubes counted for each group, ****p < 0.0001).

(P) Immunostaining of NMJs is shown (indicated by an arrow). Scale bar, 10 μm.

(Q) sEPCs were recorded from muscles co-cultured with the indicated hiMNs.

(R and S) Quantification of sEPC properties is shown (mean ± SEM; NL, n = 36; ALS1, n = 12; ALS2, n = 6; ****p < 0.0001).

See also Figures S4 and S5 and Table S2.

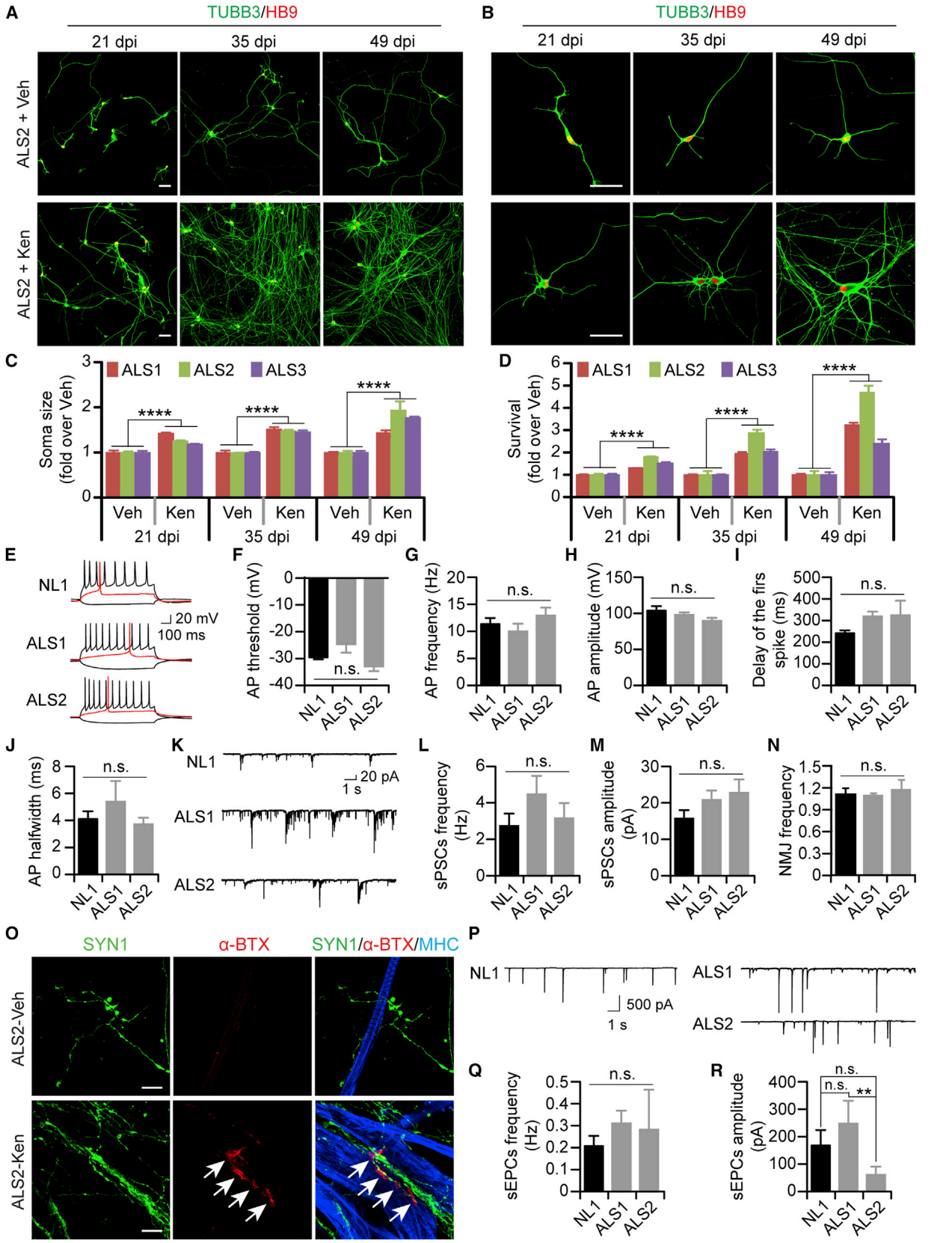

(legend on next page)

in these young neurons resemble those of disease-stage degeneration in adult human patients (Arbab et al., 2014). Our hiMN-based cellular model is complementary to the above ALS models. Parallel to iPSC-derived MNs, hiMNs harbor all the ALS-causing genetic abnormalities in human patients; yet, these cells bypass an immature embryonic stage through direct lineage reprogramming that is absent of pluripotency and stem cell proliferation (Caiazzo et al., 2011; Pang et al., 2011; Vierbuchen et al., 2010; Yoo et al., 2011). Accordingly, hiMNs may maintain age-dependent features of their parental adult cell sources, which will be critical to understanding adult-onset neurodegeneration. Thorough investigations in the future will provide more insights into the effect of direct lineage reprogramming on cell aging and neurodegeneration.

ALS hiMNs exhibit hallmarks of disease-stage degenerative MNs, including poor survival, soma shrinkage, hypoactivity, and the lack of muscle control. These deficits have been observed previously in human patient samples (Kiernan and Hudson, 1991), transgenic cellular and animal models (Bruijn et al., 1998; Gurney et al., 1994; Hadzipasic et al., 2014; Haidet-Phillips et al., 2011; Qiu et al., 2014; Re et al., 2014; Wada et al., 2012), and iPSC-derived MNs (Chen et al., 2014; Devlin et al., 2015; Kiskinis et al., 2014). Further, these hallmarks validate our hiMN-based cellular model for neurodegeneration. Nonetheless, the hypoexcitability shown by ALS hiMNs is inconsistent with the predominant excitotoxicity theory for ALS. According to this theory, the degeneration and death of patient MNs are primarily caused by their intrinsic hyperexcitability (Cleveland and Rothstein, 2001; Kuo et al., 2004; Pasinelli and Brown, 2006; Wainger et al., 2014). However, this theory is not without contradictory evidence. It was shown recently that MNs in a mutant superoxide dismutase 1 (mSOD1) mouse model of ALS are on average not hyperexcitable prior to disease onset (Delestrée et al., 2014). Leroy et al. (2014) also demonstrated that ALS-resistant, but not the ALS-vulnerable, MNs are hyperexcitable in mSOD1 mice, suggesting that early hyperexcitability is not an indicator of MN degeneration. Consistent with the pathology shown by our ALS hiMNs, some of the degenerating MNs in the mSOD1 mouse model are rather hypoexcitable (Bories et al., 2007; Delestrée et al., 2014). Most interestingly, increasing neuronal excitability is neuroprotective and ameliorates MN pathology in mSOD1 mice (Saxena et al., 2013). Therefore, hypoexcitability of affected MNs in ALS may represent a broad disease-stage endophenotype that could be targeted for therapy.

Our proof-of-concept study suggests that adult patient-specific hiMNs can be employed for drug identification and validation. ALS hiMNs are especially sensitive to systemic stresses induced by a replating procedure during culture. Significant death of hiMNs is robustly detectable within a few days under these culture conditions with or without supporting astrocytes, although co-culture with astrocytes may represent a better system that emulates an endogenous survival-promoting microenvironment for hiMNs. A pilot screen of candidate small chemical compounds identified that Ken can significantly promote ALS hiMN survival, in agreement with its previously reported neuroprotective role (Yang et al., 2013). Our further analysis also showed that Ken treatment significantly enhances dendritic outgrowth and rescues soma size of ALS hiMNs. Most importantly, our whole-cell patch-clamp recordings reveal that Ken can completely normalize ALS hiMN excitability and restore the ability to form NMJs and control muscle activity. Notwithstanding, one unsettling caveat of using Ken as a potential therapeutic drug is that hiMNs seem to be addicted to Ken treatment, such that these cells wither quickly upon drug withdrawal. Future research will be required to understand Ken-induced signaling pathways that may be specifically targeted for therapy.

In conclusion, the results of this study demonstrate that adult human skin fibroblasts can be directly and efficiently converted into highly pure and functional hiMNs through a synergistic interaction between small molecules and transcription factors. Most intriguingly, hiMNs converted from adult fibroblasts of ALS patients with FUS mutations exhibit disease-stage degenerative features that can be greatly ameliorated by the small molecule Ken. These findings reveal a unique model system that can be further exploited for understanding the molecular mechanism and the identification of therapeutics for human ALS.

EXPERIMENTAL PROCEDURES

Animals

Wild-type C57BL/6J mice were purchased from the Jackson Laboratory. All mice were housed under a 12 hr light/dark cycle and had ad libitum access to food and water in a controlled animal facility. Experimental protocols were approved by the Institutional Animal Care and Use Committee at University of Texas Southwestern.

Plasmid Construction and Virus Production

A third-generation lentiviral vector (pCSC-SP-PW-IRES-GFP) was used to express NEUROG2-IRES-GFP-T2A-SOX11, NEUROG2-IRES-SOX11, and ISL1-T2A-LHX3. YFP fusion of wild-type FUS or FUS mutants (R514G, H517Q,

Figure 7. Kenpaullone Rescues Pathophysiology of ALS hiMNs

(A and B) Kenpaullone (Ken) partially restored morphological deficits of ALS hiMNs. Representative images were taken at the indicated time points. Scale bars, 50 μm.

(C and D) Ken promoted soma size and survival of ALS hiMNs (mean ± SEM, n = 3 independent samples with ≥150 neurons analyzed for each group, ****$p < 0.0001$).

(E) Representative AP waveforms of the indicated hiMNs treated with Ken are shown.

(F–J) Ken treatment normalized electrophysiological properties of ALS hiMNs (mean ± SEM; NL1, n = 8; ALS1, n = 19; ALS2, n = 8; n.s., not significant).

(K–M) Ken enhanced sPSCs recorded from hiMNs (mean ± SEM; NL1, n = 11; ALS1, n = 17; ALS2, n = 7; n.s., not significant).

(N and O) Ken fully rescued the ability of ALS hiMNs to form NMJs (indicated by arrows) on co-cultured myotubes (mean ± SEM; n = 3 independent samples with 300 hiMN network-associated myotubes counted for each group; n.s., not significant). Scale bar, 10 μm.

(P–R) Ken enhanced sEPCs recorded from myotubes co-cultured with the indicated hiMNs (mean ± SEM; NL1, n = 8; ALS1, n = 21; ALS2, n = 10; n.s., not significant; **$p < 0.01$ when compared ALS1 and ALS2).

See also Figures S6 and S7 and Table S2.

R521C, or R522G) were gifts from Aaron Gitler (Addgene plasmid) (Sun et al., 2011) and individually sub-cloned into the pCSC-SP-PW-IRES-GFP vector by replacing the IRES-GFP cDNA fragment. Replication-incompetent lentiviruses were produced in HEK293 cells (ATCC) and stored at 4°C prior to cell transduction.

Human Fibroblast Culture

All human patient fibroblasts were obtained from the Coriell Institute for Medical Research (Table S1). They were maintained in fibroblast medium (DMEM supplemented with 15% fetal bovine serum and penicillin/streptomycin) at 37°C and 5% CO_2.

Neuron Induction and Culture

Direct lineage reprogramming was conducted according to a previous protocol with some modifications (Liu et al., 2013). In brief, fibroblasts were seeded onto Matrigel-coated culture vessels (4.8×10^5 per 24- or 48-well plate or 3×10^5 per 6-cm dish) with or without glass coverslips. Cells were transduced the next day with lentiviral supernatants in the presence of 6 μg/ml polybrene. Fibroblast culture medium was refreshed after overnight incubation. Then, 1 day later, these cells were switched to C2 medium supplemented with 10 μM FSK (Sigma-Aldrich), 1 μM DM (EMD Millipore), and 10 ng/ml FGF2 (PeproTech). The C2 medium was composed of DMEM:F12:neurobasal (2:2:1), 0.8% N2 (Invitrogen), 0.8% B27 (Invitrogen), and penicillin/streptomycin. The supplemented C2 medium was half changed every other day until 14 dpi. These cells were either directly used for analysis or further cultured after a replating procedure (Liu et al., 2013). In brief, cells were dissociated with 0.025% trypsin for 7 min at 37°C and resuspended in FBS-containing fibroblast medium to quench trypsin activity. This cell suspension was then plated onto a gelatin-coated culture dish to which fibroblasts tightly attached. About 30 min later, floating cells, which mainly consisted of induced neurons, were replated onto a new coated dish to remove residual fibroblasts, or they were directly collected by centrifugation at 500 × *g* for 2 min. Cells were resuspended into C2 medium and centrifuged again to remove cell debris. Finally, hiMNs were plated onto coated culture vessels in C2 medium supplemented with 5 μM FSK and 10 ng/ml each of BDNF, GDNF, and NT3 (PeproTech). Unless indicated otherwise, C2 media with neurotrophic factors were half changed twice a week.

Immunofluorescence, BrdU Labeling, and Cell Counting

Cell cultures at the indicated time points were fixed with 4% paraformaldehyde (PFA) in PBS for 15 min at room temperature, and they were permeabilized/blocked for 1 hr in blocking solution (1× PBS containing 0.2% Triton X-100 and 3% BSA). Cells were then processed for immunocytochemistry as previously described (Liu et al., 2013). For subcellular distribution of FUS, confocal images were obtained with a NIKON A1R Confocal Microscope. The total fluorescence intensity of FUS staining in the nucleus or soma was quantified separately using ImageJ with a plugin of ND to Image6D. The cytosolic FUS staining was calculated by subtracting nuclear fluorescence intensity from that of the soma. The relative subcellular distribution of FUS was expressed as the ratio of nuclear/cytoplasmic fluorescence intensity. For experimental details, please see the Supplemental Experimental Procedures.

Western Blot Analysis

Whole-cell lysates were obtained through direct lysis of cells in 50 mM Tris-HCl buffer (pH 8.0) containing 150 mM NaCl, 1% NP40, 1% Triton X-100, 0.1% SDS, 0.5% sodium deoxycholate, and protease inhibitor cocktail (Roche). Equal amounts of these lysates (20 μg per lane) were used for SDS-PAGE and western blot analysis as previously described (Kwiatkowski et al., 2009). The blots were probed with either a goat anti-FUS (Bethyl Laboratories, 1:5,000) or a mouse anti-actin (Jackson Laboratory, 1:10,000) antibody, followed by their corresponding HRP-conjugated secondary antibodies. After visualization with the ECL substrate, densitometric analysis was performed using the ImageJ software. The relative expression of ectopic and endogenous FUS proteins was obtained after normalizing to the loading control actin.

Survival and Morphometric Analysis

The hiMNs co-cultured with primary mouse astrocytes were used for these analyses. Cortical astrocytes were prepared from post-natal day (P)1–P3 mouse pups as previously described (Vierbuchen et al., 2010). Endogenous mouse neurons were removed by vigorous shaking and a few cycles of passaging, freezing, thawing, and plating. The hiMNs at 14 dpi were replated on astrocyte-coated 96-well plates (for survival analysis) or coverslip-containing 24-well plates (for soma size analysis). Co-cultures were fed twice a week with C2 medium containing 5 μM FSK and 10 ng/ml each of BDNF, GDNF, and NT3. Cells were fixed and immunostained for TUBB3 and GFP at the indicated time points. Under an AMG EVOS digital inverted fluorescence microscope, $TUBB3^+GFP^+$ cells within the entire well of a 96-well plate in triplicate were manually quantified by a researcher blinded to experimental groups. Cell counts were normalized to the starting number of cells plated into each well. To determine the survival rate, a similar number of starting cells were plated and counted at 14, 21, 35, and 49 dpi. Survival rate at 14 dpi for each line was set as 100%, to which the subsequent survived cells at each time point were normalized. To facilitate comparison between different lines, a relative survival rate was calculated by further normalization to NL1 at each time point.

The hiMNs on glass coverslips were used for measuring soma size. $TUBB3^+GFP^+$ cells from triplicate samples were randomly selected and imaged with an Olympus BX51 Microscope equipped with StereoInvestigator software. Soma area was outlined and measured with the vendor-provided software. For experiments with ectopic FUS expression, a plasmid without the GFP tag NEUROG2-IRES-SOX1 was used for reprogramming. As such, only YFP (empty vector) or YFP-tagged wild-type or mutant FUS was measured. A similar number of YFP-expressing cells were plated and counted at 14 and 21 dpi. A survival rate was obtained by normalizing the cell number at 21 dpi to that at 14 dpi. This was further normalized to the empty vector control group (Vector) to facilitate comparisons between groups.

Neuron and Muscle Co-cultures

Primary skeletal myoblasts from P0–P1 mouse pups were isolated and differentiated into myotubes as previously described with modifications (Nelson et al., 2013). Briefly, neonatal limb muscles were collected into ice-cold HBSS under a dissecting microscope and digested with 0.2% collagenase II and 1,000 U/ml DNase I for 45 min at 37°C. Dissociated myoblasts were expanded in 1% gelatin-coated dishes for 2–4 days in culture medium (DMEM containing 10% horse serum, 5% newborn calf serum, and 1% chick embryo extracts), and then they were induced to form multinucleated myotubes by switching to differentiation medium (DMEM containing 2% horse serum). Then, 24 hr later, 10 μM cytosine arabinoside (AraC) was added to the culture medium to stop proliferation of undifferentiated cells. After another day, the cells were dissociated with 0.05% trypsin for 5 min at 37°C. Trypsin was inhibited by adding culture medium and removed by centrifugation at 500 × *g* for 2 min. The myotubes were resuspended in C2 medium containing 10 ng/ml each of BDNF, GDNF, and NT3, and then they were plated onto coverslips covered with astrocytes and hiMNs at 46 to 49 dpi. A majority of myotubes started rhythmic contractions 2–3 days in co-cultures with hiMNs. These cells at 4–7 days in co-culture were used for examination of NMJs and electrophysiology. NMJs were visualized by confocal laser-scanning microscopy after labeling with rhodamine-conjugated α-BTX (Invitrogen, 1:500) and immunostaining of TUBB3 (Covance, 1:5,000), synapsin1 (Cell Signaling Technology, 1:500), and MHC (Sigma, 1:1,000). NMJ formation frequency was determined by the number of NMJs on >300 myotubes associated with hiMN networks.

Electrophysiology

Whole-cell patch-clamp recordings were performed under visual guidance using infra-red differential interference contrast (IR-DIC) and GFP fluorescence, as previously described (Liu et al., 2013). For experimental details, please see the Supplemental Experimental Procedures.

Statistical Analysis

All experiments were performed at least twice in triplicate unless otherwise indicated. Data are presented as mean ± SEM. Statistical analysis was done in GraphPad Prism. The D'Agostino & Pearson omnibus normality test was first done on the data to determine whether it was normal distribution. If data passed the normality test, then one-way or two-way ANOVA was used to

determine significance. If data did not pass the normality test, then the Kruskal-Wallis test was used to determine significance. A two-sample two-sided Kolmogorov-Smirnov test in R (R Project, Bell Laboratories) was used for cumulative probability analysis. Significant differences are indicated by *$p < 0.05$, **$p < 0.01$, ***$p < 0.001$, and ****$p < 0.0001$.

SUPPLEMENTAL INFORMATION

Supplemental Information includes Supplemental Experimental Procedures, seven figures, and two tables and can be found with this article online at http://dx.doi.org/10.1016/j.celrep.2015.12.018.

AUTHOR CONTRIBUTIONS

M.-L.L., T.Z., and C.-L.Z. conceived and designed the experiments. M.-L.L. performed all experiments related to molecular and cellular biology and T.Z. conducted all experiments related to electrophysiology. M.-L.L., T.Z., and C.-L.Z. prepared the manuscript.

ACKNOWLEDGMENTS

We thank members of the C.-L.Z. laboratory for discussions and reagents and Dr. Weichun Lin (UT Southwestern) for advice on NMJs. C.-L.Z. is a W.W. Caruth, Jr. Scholar in Biomedical Research. This work was supported by the Welch Foundation Award (I-1724), the Decherd Foundation, the Ellison Medical Foundation (AG-NS-0753-11), and NIH grants (R01NS070981, R01NS088095, and R21NS093502 to C.-L.Z.).

Received: May 12, 2015
Revised: October 17, 2015
Accepted: November 23, 2015
Published: December 24, 2015

REFERENCES

Arbab, M., Baars, S., and Geijsen, N. (2014). Modeling motor neuron disease: the matter of time. Trends Neurosci. *37*, 642–652.

Bergemalm, D., Jonsson, P.A., Graffmo, K.S., Andersen, P.M., Brännström, T., Rehnmark, A., and Marklund, S.L. (2006). Overloading of stable and exclusion of unstable human superoxide dismutase-1 variants in mitochondria of murine amyotrophic lateral sclerosis models. J. Neurosci. *26*, 4147–4154.

Bories, C., Amendola, J., Lamotte d'Incamps, B., and Durand, J. (2007). Early electrophysiological abnormalities in lumbar motoneurons in a transgenic mouse model of amyotrophic lateral sclerosis. Eur. J. Neurosci. *25*, 451–459.

Bruijn, L.I., Houseweart, M.K., Kato, S., Anderson, K.L., Anderson, S.D., Ohama, E., Reaume, A.G., Scott, R.W., and Cleveland, D.W. (1998). Aggregation and motor neuron toxicity of an ALS-linked SOD1 mutant independent from wild-type SOD1. Science *281*, 1851–1854.

Caiazzo, M., Dell'Anno, M.T., Dvoretskova, E., Lazarevic, D., Taverna, S., Leo, D., Sotnikova, T.D., Menegon, A., Roncaglia, P., Colciago, G., et al. (2011). Direct generation of functional dopaminergic neurons from mouse and human fibroblasts. Nature *476*, 224–227.

Chen, H., Qian, K., Du, Z., Cao, J., Petersen, A., Liu, H., Blackbourn, L.W., 4th, Huang, C.L., Errigo, A., Yin, Y., et al. (2014). Modeling ALS with iPSCs reveals that mutant SOD1 misregulates neurofilament balance in motor neurons. Cell Stem Cell *14*, 796–809.

Cleveland, D.W., and Rothstein, J.D. (2001). From Charcot to Lou Gehrig: deciphering selective motor neuron death in ALS. Nat. Rev. Neurosci. *2*, 806–819.

Corrado, L., Del Bo, R., Castellotti, B., Ratti, A., Cereda, C., Penco, S., Sorarù, G., Carlomagno, Y., Ghezzi, S., Pensato, V., et al. (2010). Mutations of FUS gene in sporadic amyotrophic lateral sclerosis. J. Med. Genet. *47*, 190–194.

Delestrée, N., Manuel, M., Iglesias, C., Elbasiouny, S.M., Heckman, C.J., and Zytnicki, D. (2014). Adult spinal motoneurones are not hyperexcitable in a mouse model of inherited amyotrophic lateral sclerosis. J. Physiol. *592*, 1687–1703.

Detmer, S.A., Vande Velde, C., Cleveland, D.W., and Chan, D.C. (2008). Hindlimb gait defects due to motor axon loss and reduced distal muscles in a transgenic mouse model of Charcot-Marie-Tooth type 2A. Hum. Mol. Genet. *17*, 367–375.

Devlin, A.C., Burr, K., Borooah, S., Foster, J.D., Cleary, E.M., Geti, I., Vallier, L., Shaw, C.E., Chandran, S., and Miles, G.B. (2015). Human iPSC-derived motoneurons harbouring TARDBP or C9ORF72 ALS mutations are dysfunctional despite maintaining viability. Nat. Commun. *6*, 5999.

Dimos, J.T., Rodolfa, K.T., Niakan, K.K., Weisenthal, L.M., Mitsumoto, H., Chung, W., Croft, G.F., Saphier, G., Leibel, R., Goland, R., et al. (2008). Induced pluripotent stem cells generated from patients with ALS can be differentiated into motor neurons. Science *321*, 1218–1221.

Gladman, M., Cudkowicz, M., and Zinman, L. (2012). Enhancing clinical trials in neurodegenerative disorders: lessons from amyotrophic lateral sclerosis. Curr. Opin. Neurol. *25*, 735–742.

Gurney, M.E., Pu, H., Chiu, A.Y., Dal Canto, M.C., Polchow, C.Y., Alexander, D.D., Caliendo, J., Hentati, A., Kwon, Y.W., Deng, H.X., et al. (1994). Motor neuron degeneration in mice that express a human Cu,Zn superoxide dismutase mutation. Science *264*, 1772–1775.

Hadzipasic, M., Tahvildari, B., Nagy, M., Bian, M., Horwich, A.L., and McCormick, D.A. (2014). Selective degeneration of a physiological subtype of spinal motor neuron in mice with SOD1-linked ALS. Proc. Natl. Acad. Sci. USA *111*, 16883–16888.

Haidet-Phillips, A.M., Hester, M.E., Miranda, C.J., Meyer, K., Braun, L., Frakes, A., Song, S., Likhite, S., Murtha, M.J., Foust, K.D., et al. (2011). Astrocytes from familial and sporadic ALS patients are toxic to motor neurons. Nat. Biotechnol. *29*, 824–828.

Howland, D.S., Liu, J., She, Y., Goad, B., Maragakis, N.J., Kim, B., Erickson, J., Kulik, J., DeVito, L., Psaltis, G., et al. (2002). Focal loss of the glutamate transporter EAAT2 in a transgenic rat model of SOD1 mutant-mediated amyotrophic lateral sclerosis (ALS). Proc. Natl. Acad. Sci. USA *99*, 1604–1609.

Julien, J.P., and Kriz, J. (2006). Transgenic mouse models of amyotrophic lateral sclerosis. Biochim. Biophys. Acta *1762*, 1013–1024.

Kiernan, J.A., and Hudson, A.J. (1991). Changes in sizes of cortical and lower motor neurons in amyotrophic lateral sclerosis. Brain *114*, 843–853.

Kimchi-Sarfaty, C., Oh, J.M., Kim, I.W., Sauna, Z.E., Calcagno, A.M., Ambudkar, S.V., and Gottesman, M.M. (2007). A "silent" polymorphism in the MDR1 gene changes substrate specificity. Science *315*, 525–528.

Kiskinis, E., Sandoe, J., Williams, L.A., Boulting, G.L., Moccia, R., Wainger, B.J., Han, S., Peng, T., Thams, S., Mikkilineni, S., et al. (2014). Pathways disrupted in human ALS motor neurons identified through genetic correction of mutant SOD1. Cell Stem Cell *14*, 781–795.

Kuo, J.J., Schonewille, M., Siddique, T., Schults, A.N., Fu, R., Bär, P.R., Anelli, R., Heckman, C.J., and Kroese, A.B. (2004). Hyperexcitability of cultured spinal motoneurons from presymptomatic ALS mice. J. Neurophysiol. *91*, 571–575.

Kwiatkowski, T.J., Jr., Bosco, D.A., Leclerc, A.L., Tamrazian, E., Vanderburg, C.R., Russ, C., Davis, A., Gilchrist, J., Kasarskis, E.J., Munsat, T., et al. (2009). Mutations in the FUS/TLS gene on chromosome 16 cause familial amyotrophic lateral sclerosis. Science *323*, 1205–1208.

Lai, S.L., Abramzon, Y., Schymick, J.C., Stephan, D.A., Dunckley, T., Dillman, A., Cookson, M., Calvo, A., Battistini, S., Giannini, F., et al.; ITALSGEN Consortium (2011). FUS mutations in sporadic amyotrophic lateral sclerosis. Neurobiol. Aging *32*, 550.e1–550.e4.

Lapasset, L., Milhavet, O., Prieur, A., Besnard, E., Babled, A., Aït-Hamou, N., Leschik, J., Pellestor, F., Ramirez, J.M., De Vos, J., et al. (2011). Rejuvenating senescent and centenarian human cells by reprogramming through the pluripotent state. Genes Dev. *25*, 2248–2253.

Lee, S., Cuvillier, J.M., Lee, B., Shen, R., Lee, J.W., and Lee, S.K. (2012). Fusion protein Isl1-Lhx3 specifies motor neuron fate by inducing motor neuron genes and concomitantly suppressing the interneuron programs. Proc. Natl. Acad. Sci. USA *109*, 3383–3388.

Leng, Y., Liang, M.H., Ren, M., Marinova, Z., Leeds, P., and Chuang, D.M. (2008). Synergistic neuroprotective effects of lithium and valproic acid or other histone deacetylase inhibitors in neurons: roles of glycogen synthase kinase-3 inhibition. J. Neurosci. *28*, 2576–2588.

Leroy, F., Lamotte d'Incamps, B., Imhoff-Manuel, R.D., and Zytnicki, D. (2014). Early intrinsic hyperexcitability does not contribute to motoneuron degeneration in amyotrophic lateral sclerosis. eLife *3*, e04046.

Liu, M.L., Zang, T., Zou, Y., Chang, J.C., Gibson, J.R., Huber, K.M., and Zhang, C.L. (2013). Small molecules enable neurogenin 2 to efficiently convert human fibroblasts into cholinergic neurons. Nat. Commun. *4*, 2183.

Miller, J.D., Ganat, Y.M., Kishinevsky, S., Bowman, R.L., Liu, B., Tu, E.Y., Mandal, P.K., Vera, E., Shim, J.W., Kriks, S., et al. (2013). Human iPSC-based modeling of late-onset disease via progerin-induced aging. Cell Stem Cell *13*, 691–705.

Musarò, A. (2013). Understanding ALS: new therapeutic approaches. FEBS J. *280*, 4315–4322.

Nelson, B.R., Wu, F., Liu, Y., Anderson, D.M., McAnally, J., Lin, W., Cannon, S.C., Bassel-Duby, R., and Olson, E.N. (2013). Skeletal muscle-specific T-tubule protein STAC3 mediates voltage-induced Ca2+ release and contractility. Proc. Natl. Acad. Sci. USA *110*, 11881–11886.

Niu, W., Zang, T., Zou, Y., Fang, S., Smith, D.K., Bachoo, R., and Zhang, C.L. (2013). In vivo reprogramming of astrocytes to neuroblasts in the adult brain. Nat. Cell Biol. *15*, 1164–1175.

Pang, Z.P., Yang, N., Vierbuchen, T., Ostermeier, A., Fuentes, D.R., Yang, T.Q., Citri, A., Sebastiano, V., Marro, S., Südhof, T.C., and Wernig, M. (2011). Induction of human neuronal cells by defined transcription factors. Nature *476*, 220–223.

Pasinelli, P., and Brown, R.H. (2006). Molecular biology of amyotrophic lateral sclerosis: insights from genetics. Nat. Rev. Neurosci. *7*, 710–723.

Pieper, A.A., Xie, S., Capota, E., Estill, S.J., Zhong, J., Long, J.M., Becker, G.L., Huntington, P., Goldman, S.E., Shen, C.H., et al. (2010). Discovery of a proneurogenic, neuroprotective chemical. Cell *142*, 39–51.

Qiu, H., Lee, S., Shang, Y., Wang, W.Y., Au, K.F., Kamiya, S., Barmada, S.J., Finkbeiner, S., Lui, H., Carlton, C.E., et al. (2014). ALS-associated mutation FUS-R521C causes DNA damage and RNA splicing defects. J. Clin. Invest. *124*, 981–999.

Rando, T.A., and Chang, H.Y. (2012). Aging, rejuvenation, and epigenetic reprogramming: resetting the aging clock. Cell *148*, 46–57.

Re, D.B., Le Verche, V., Yu, C., Amoroso, M.W., Politi, K.A., Phani, S., Ikiz, B., Hoffmann, L., Koolen, M., Nagata, T., et al. (2014). Necroptosis drives motor neuron death in models of both sporadic and familial ALS. Neuron *81*, 1001–1008.

Robberecht, W., and Philips, T. (2013). The changing scene of amyotrophic lateral sclerosis. Nat. Rev. Neurosci. *14*, 248–264.

Rosen, D.R. (1993). Mutations in Cu/Zn superoxide dismutase gene are associated with familial amyotrophic lateral sclerosis. Nature *364*, 362.

Ryan, S.D., Dolatabadi, N., Chan, S.F., Zhang, X., Akhtar, M.W., Parker, J., Soldner, F., Sunico, C.R., Nagar, S., Talantova, M., et al. (2013). Isogenic human iPSC Parkinson's model shows nitrosative stress-induced dysfunction in MEF2-PGC1α transcription. Cell *155*, 1351–1364.

Saxena, S., Roselli, F., Singh, K., Leptien, K., Julien, J.P., Gros-Louis, F., and Caroni, P. (2013). Neuroprotection through excitability and mTOR required in ALS motoneurons to delay disease and extend survival. Neuron *80*, 80–96.

Son, E.Y., Ichida, J.K., Wainger, B.J., Toma, J.S., Rafuse, V.F., Woolf, C.J., and Eggan, K. (2011). Conversion of mouse and human fibroblasts into functional spinal motor neurons. Cell Stem Cell *9*, 205–218.

Spalloni, A., Origlia, N., Sgobio, C., Trabalza, A., Nutini, M., Berretta, N., Bernardi, G., Domenici, L., Ammassari-Teule, M., and Longone, P. (2011). Postsynaptic alteration of NR2A subunit and defective autophosphorylation of alphaCaMKII at threonine-286 contribute to abnormal plasticity and morphology of upper motor neurons in presymptomatic SOD1G93A mice, a murine model for amyotrophic lateral sclerosis. Cereb. Cortex *21*, 796–805.

Sreedharan, J., Blair, I.P., Tripathi, V.B., Hu, X., Vance, C., Rogelj, B., Ackerley, S., Durnall, J.C., Williams, K.L., Buratti, E., et al. (2008). TDP-43 mutations in familial and sporadic amyotrophic lateral sclerosis. Science *319*, 1668–1672.

Sun, Z., Diaz, Z., Fang, X., Hart, M.P., Chesi, A., Shorter, J., and Gitler, A.D. (2011). Molecular determinants and genetic modifiers of aggregation and toxicity for the ALS disease protein FUS/TLS. PLoS Biol. *9*, e1000614.

Thaler, J.P., Lee, S.K., Jurata, L.W., Gill, G.N., and Pfaff, S.L. (2002). LIM factor Lhx3 contributes to the specification of motor neuron and interneuron identity through cell-type-specific protein-protein interactions. Cell *110*, 237–249.

Vance, C., Rogelj, B., Hortobágyi, T., De Vos, K.J., Nishimura, A.L., Sreedharan, J., Hu, X., Smith, B., Ruddy, D., Wright, P., et al. (2009). Mutations in FUS, an RNA processing protein, cause familial amyotrophic lateral sclerosis type 6. Science *323*, 1208–1211.

Victor, M.B., Richner, M., Hermanstyne, T.O., Ransdell, J.L., Sobieski, C., Deng, P.Y., Klyachko, V.A., Nerbonne, J.M., and Yoo, A.S. (2014). Generation of human striatal neurons by microRNA-dependent direct conversion of fibroblasts. Neuron *84*, 311–323.

Vierbuchen, T., Ostermeier, A., Pang, Z.P., Kokubu, Y., Südhof, T.C., and Wernig, M. (2010). Direct conversion of fibroblasts to functional neurons by defined factors. Nature *463*, 1035–1041.

Wada, T., Goparaju, S.K., Tooi, N., Inoue, H., Takahashi, R., Nakatsuji, N., and Aiba, K. (2012). Amyotrophic lateral sclerosis model derived from human embryonic stem cells overexpressing mutant superoxide dismutase 1. Stem Cells Transl. Med. *1*, 396–402.

Wainger, B.J., Kiskinis, E., Mellin, C., Wiskow, O., Han, S.S., Sandoe, J., Perez, N.P., Williams, L.A., Lee, S., Boulting, G., et al. (2014). Intrinsic membrane hyperexcitability of amyotrophic lateral sclerosis patient-derived motor neurons. Cell Rep. *7*, 1–11.

Wainger, B.J., Buttermore, E.D., Oliveira, J.T., Mellin, C., Lee, S., Saber, W.A., Wang, A.J., Ichida, J.K., Chiu, I.M., Barrett, L., et al. (2015). Modeling pain in vitro using nociceptor neurons reprogrammed from fibroblasts. Nat. Neurosci. *18*, 17–24.

Yang, Y.M., Gupta, S.K., Kim, K.J., Powers, B.E., Cerqueira, A., Wainger, B.J., Ngo, H.D., Rosowski, K.A., Schein, P.A., Ackeifi, C.A., et al. (2013). A small molecule screen in stem-cell-derived motor neurons identifies a kinase inhibitor as a candidate therapeutic for ALS. Cell Stem Cell *12*, 713–726.

Yoo, A.S., Sun, A.X., Li, L., Shcheglovitov, A., Portmann, T., Li, Y., Lee-Messer, C., Dolmetsch, R.E., Tsien, R.W., and Crabtree, G.R. (2011). MicroRNA-mediated conversion of human fibroblasts to neurons. Nature *476*, 228–231.

Yu, C.H., Dang, Y., Zhou, Z., Wu, C., Zhao, F., Sachs, M.S., and Liu, Y. (2015). Codon Usage Influences the Local Rate of Translation Elongation to Regulate Co-translational Protein Folding. Mol. Cell *59*, 744–754.

Zhou, M., Guo, J., Cha, J., Chae, M., Chen, S., Barral, J.M., Sachs, M.S., and Liu, Y. (2013). Non-optimal codon usage affects expression, structure and function of clock protein FRQ. Nature *495*, 111–115.

Zhou, M., Wang, T., Fu, J., Xiao, G., and Liu, Y. (2015). Nonoptimal codon usage influences protein structure in intrinsically disordered regions. Mol. Microbiol. *97*, 974–987.